

Dear author,

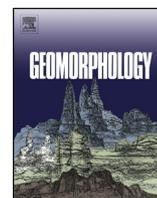
Please note that changes made in the online proofing system will be added to the article before publication but are not reflected in this PDF.

We also ask that this file not be used for submitting corrections.



Contents lists available at ScienceDirect

Geomorphology

journal homepage: [www.elsevier.com/locate/geomorph](http://www.elsevier.com/locate/geomorph)

## Q4 Forensic investigations of the Cima Salti Landslide, northern Italy, using 2 runout simulations

Q6 Q5 Margherita Cecilia Spreafico <sup>a</sup>, Andrea Wolter <sup>b,\*</sup>, Vincenzo Picotti <sup>b</sup>, Lisa Borgatti <sup>a</sup>,  
4 Anne Mangeney <sup>c,d</sup>, Monica Ghirotti <sup>e</sup>

5 <sup>a</sup> Department of Civil, Chemical, Environmental, and Materials Engineering, Università di Bologna, Bologna, Italy

6 <sup>b</sup> Department of Earth Sciences, ETH Zürich, Zürich, Switzerland

7 <sup>c</sup> Université Paris Diderot, Sorbonne Paris Cité, Institut de Physique du Globe de Paris, Seismology Group, Paris, France

8 <sup>d</sup> ANGE Team, INRIA, Lab. J.-L. Lions, UPMC, Paris, France

9 <sup>e</sup> Department of Physics and Earth Sciences, Università degli Studi di Ferrara, Ferrara, Italy

### 1 1 A R T I C L E I N F O

#### 12 Article history:

13 Received 17 January 2018

14 Received in revised form 26 April 2018

15 Accepted 27 April 2018

16 Available online xxx

#### 20

#### 35 Keywords:

36 Cima Salti rock avalanche

37 Runout simulations

38 Valley evolution

39 DAN3D

40 SHALTOP

### A B S T R A C T

Over the last decades, a movement has begun to reclassify deposits previously misidentified as having origins 22 other than landsliding. The reverse problem of incorrectly assigning deposits a mass movement origin, however, 23 has been addressed less in the landslide community. The Cima Salti Landslide in the Lake Garda region of 24 Northern Italy is a cautionary tale of assuming source areas and volumes. It was traditionally thought to have 25 dammed Tenno Lake in the Middle Ages, and to have a volume of 20–30 Mm<sup>3</sup>. We show through geological 26 field data and simple runout simulations with the codes DAN3D and SHALTOP (which produced comparable 27 results) that the volume of the landslide was likely significantly overestimated in the past, and that it most likely 28 did not dam Tenno Lake, as has been assumed. We propose that a smaller volume landslide (2–5 ) was deposited 29 on stagnant ice melting in situ in the Lateglacial period, a relatively minor event in the complex history of the 30 Magnone valley. This interpretation emphasizes the importance of careful field investigations and assumption 31 validation, at Cima Salti and in a broader context. It also shows the unique capacity of landslide simulation to 32 guide field observation and discriminate mass emplacement processes. 33

© 2017 Published by Elsevier B.V. 34

#### 42

#### 43

### Q8 1. Introduction and setting

46 Over the last few decades, landslide research has focused on exposing 47 and highlighting material that had previously been classified as having 48 other origins, expanding the global inventory of landslides (cf. Hart 49 et al., 2012; Reznichenko et al., 2012; Reznichenko and Davies, 2015; 50 Schleier et al., 2015). Assumed landslides, however, have also been 51 misidentified and misrepresented (McCull and Davies, 2011; Brunet 52 et al., 2016, 2017), with implications for hazard assessment. In this 53 paper, we present the cautionary tale of the Cima Salti Landslide in 54 Northern Italy, that was hypothesized to be responsible for the formation 55 of Tenno Lake. Our aim is to expand the understanding of the landslide 56 within the context of the evolution of the Magnone valley, and to deter- 57 mine, ultimately, how Tenno Lake was dammed. The paper addresses 58 first the geomorphic and geological context of the landslide as well as 59 methods applied to investigate it, then summarises the results of runout 60 simulations of volume considerations and glacier presence and absence.

The Cima Salti Landslide is situated north of Lake Garda in the 61 Trentino region of Italy. It has an obvious headscarp with a crown at 62 approximately 1220 m asl on the NE slope of Cima Salti, but the lower 63 limit of the depletion zone and the extent of the deposit are not clear. 64 The Fahrböschung of the landslide is 21.8°. Talus covers most of 65 the slope at present, and this material locally remobilised during a 66 rotational sliding event in 2000. After this recent event, the slope was 67 further altered by stabilization works (Fig. 1). 68

The Magnone valley has a complex history (Fig. 2). It is dissected by 69 reverse and transpressive faults, including two NNE-striking reverse 70 faults in the crown area of the landslide. The valley is divided by the 71 Ballino line, a major transpressional fault that inverted a previous rift 72 structure, separating two distinct Mesozoic facies (Castellarin and 73 Picotti, 1990). The peak of Cima Salti comprises bedded, high-strength 74 (Uniaxial Compressive Strength, UCS = 100–200 MPa, estimated in 75 the field) Maiolica Fm limestones (Uppermost Jurassic to Lower 76 Cretaceous) crosscut by two discontinuity sets and several faults, with 77 the underlying Selcifero Lombardo Fm radiolarites (Middle to Upper 78 Jurassic) and Tofino Fm cherty limestones (Lower to Middle Jurassic) 79 downslope (Fig. 3). 80

\* Corresponding author.  
E-mail address: [awolter@sfcu.ca](mailto:awolter@sfcu.ca) (A. Wolter).

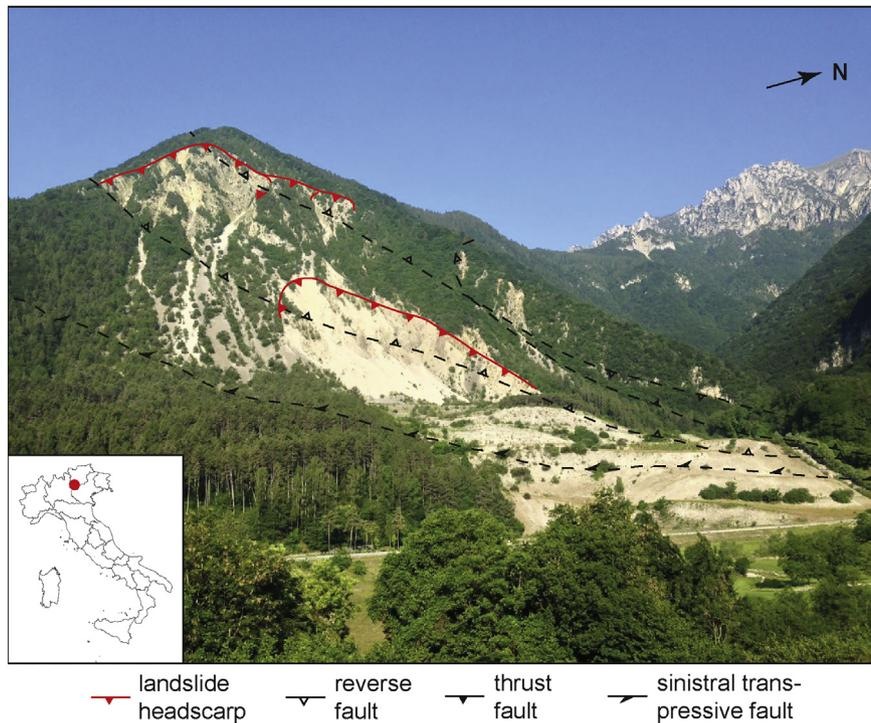


**Fig. 1.** View of the Cima Salti slope in northern Italy. The upper headscarp is the Cima Salti landslide scarp, the lower the 2000 event. Faults after Picotti (2003). Image taken by authors (June 2017).

81 During the Pleniglacial, a branch of the main Adamello-Adige-Garda  
82 glacier flowed to the south over the Ballino transfluence saddle, located  
83 just north of Tenno Lake. In the Lateglacial age, this transfluence was  
84 deactivated and the Magnone valley was obstructed by a shallower ice  
85 tongue flowing north. During its retreat, this glacier deposited several  
86 orders of sinuated moraines, the most continuous of these at the base  
87 of Cima Salti and south of Tenno Lake. Erosional remnants of lake

88 sediments have been found at elevations decreasing from approxi-  
89 mately 740 to 600 m asl in the area, suggesting multiple ice-contact  
90 lakes (Picotti, 2003).

91 Considering the regional context, several large rock avalanches  
92 affected the Trentino region during the Lateglacial and the Holocene,  
93 contributing significantly to landscape evolution in the area (Fuganti,  
94 1969; Perna, 1974; Chinaglia, 1993; Bassetti, 1997). For example, in

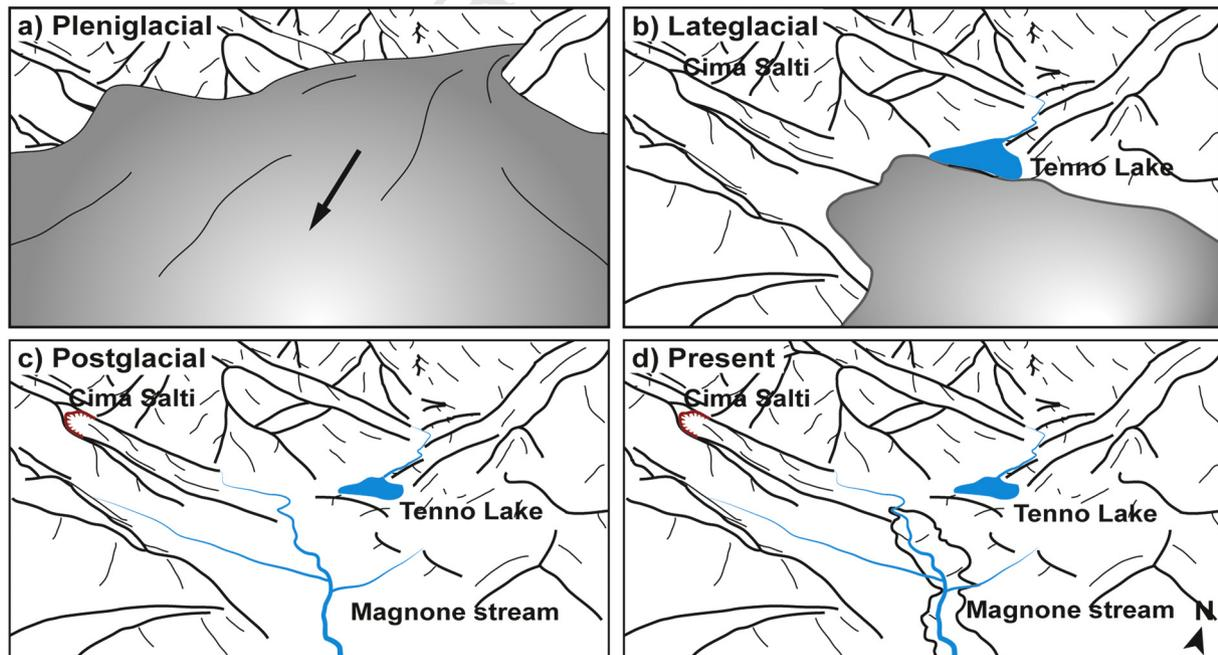


**Fig. 2.** Evolution of the landscape in the Cima Salti area. a) Pleniglacial ice flowing to the south. b) Lateglacial ice coming from the south. c) Postglacial landscape with headscarp of the landslide in red. d) Present topography with the incision of the Magnone stream. (For interpretation of the references to colour in this figure legend, the reader is referred to the web version of this article.)

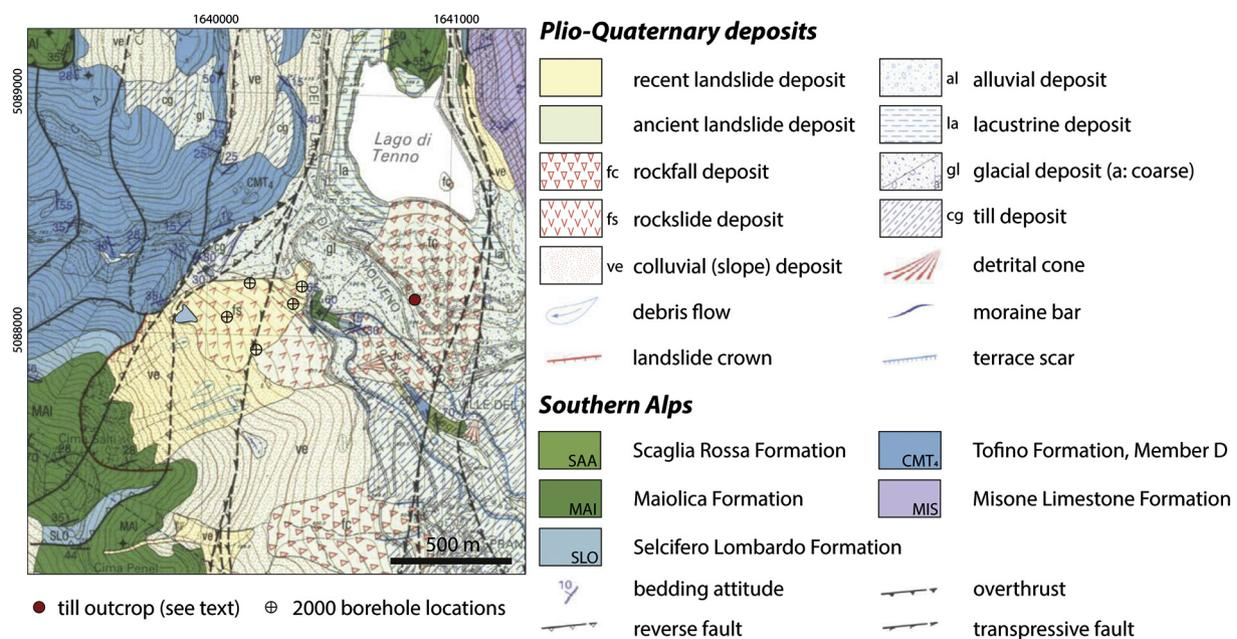


**Fig. 3.** Geological map of the Cima Salti area, modified after Picotti and Tommasi (2002). Till outcrop refers to the outcrop described in the text. Coordinates are in the UTM Sistema Geodetico Nazionale (ROMA, 1940).

Q1

95 the Sarca valley large deposits comprising limestone megaboulders,  
 96 known as “Marocche”, can be found (Trenner, 1924; Perna, 1974;  
 97 Chinaglia, 1993; Bassetti, 1997). Trenner (1924) recognised three large  
 98 landslides and nine small events. Based on the finding of Roman relics,  
 99 he suggested a post-Roman age for at least one of them. More recently,  
 100 Perna (1974) dated the “Marocche” deposits using paleo-karst features  
 101 to post-Last Glacial Maximum. Bassetti (1997) identified six landslides  
 102 and found Bronze Age materials within the deposits, and suggested an  
 103 historical age. Based on  $^{36}\text{Cl}$  exposure dating of carbonate megaboulders,  
 104 Ivy-Ochs et al. (2017) dated the main “Marocche” rock avalanches to  
 105 around 5000 years BP. Two periods of enhanced landslide activity  
 106 followed: one around 1600 years BP (late Roman Age) and one Medieval,  
 107 which may have been triggered by the 1117 CE Verona Earthquake  
 108 (Guidoboni et al., 2005). The Lavini di Marco rock avalanche (Orombelli  
 109 and Sauro, 1988; Tommasi et al., 2009), whose deposit dammed and  
 110 deviated the Adige River, was supposedly triggered by this earthquake  
 111 (Guidoboni et al., 2005; Galadini et al., 2001: 1040–1215 CE). Recently,  
 112 however, Martin et al. (2014) showed that the Lavini di Marco rockslide  
 113 deposit dates to  $3000 \pm 400$  years BP. Some ages on the sliding plane  
 114 record small-scale reactivations; a single age of  $800 \pm 210$  years suggests  
 115 a reactivation at Lavini di Marco coincident with the Verona earthquake.  
 116 Galadini et al. (2001) related the Cima Salti Landslide to the same seismic  
 117 event.

118 Several previous authors, including Dalla Torre (1913), Venzo  
 119 (1935), Tommasi (1963), Vaia (1981), and Pirocchi (1992), have  
 120 assumed that Tenno Lake, located at the NE border of the landslide  
 121 at 570 m asl with a current maximum depth of 47.7 m and an area of  
 122  $0.22 \text{ km}^2$  (APPA, Trento Province, 2017), was dammed by the Cima  
 123 Salti Landslide, and that the topographic high in the centre of the  
 124 Magnone valley comprises the landslide deposit. Relatively young  
 125 radiocarbon ages (950–1380 CE) of submerged trees in the lake seem  
 126 to support their theory of a 1300 CE event (Alessio et al., 1973). Penck  
 127 and Brückner (1909), Picotti and Tommasi (2002), Picotti (2003), and  
 128 Ghirotti et al. (2015), however, interpreted most of the surficial material  
 129 as till, based on field observations. Outcrops are extremely limited in  
 130 number due to vegetation cover and anthropic reworking of material.  
 131 Nonetheless, one small outcrop in the centre of the valley (see Fig. 3)  
 132 indicates lodgment till overlying pre-Quaternary bedrock, with 40%  
 133 reddish-brown silty matrix surrounding, 60% polymictic clasts (cm to  
 134 dm scale) and underlying 30 cm of brownish soil. Boreholes drilled on

the Cima Salti flank in 2001–2002 show 30–60 m of gravel assumed to  
 be pre-2000 landslide debris overlying up to 30 m thick dark clayey  
 silts assumed to be lacustrine deposits in direct contact with bedrock.  
 The clayey silts were absent toward the lake. Unfortunately, no  
 boreholes were drilled outside the 2000 landslide extent, and hence  
 conclusions about the centre of the valley are limited to isolated  
 outcrops of till. Critical in distinguishing till from landslide deposits is  
 lithology (texture, origin and shape of clasts) and degree of induration,  
 weathering and fragmentation. The till deposits in the area are polymictic  
 and tend to be matrix-supported, whereas the landslide deposits com-  
 prise solely Maiolica blocks and are clast-supported. According to Penck  
 and Brückner (1909), Picotti and Tommasi (2002), Picotti (2003), and  
 Ghirotti et al. (2015), the ridge damming the modern Tenno Lake consists  
 of a rock drumlin covered with the ablation till of the Lateglacial moraine  
 and partially with Maiolica blocks, deriving from the Cima Salti event.  
 The submerged trees in the lake, in the opinion of these latter authors, could  
 indicate later fluctuations in the lake levels.

The Cima Salti Landslide, therefore, may not have changed the valley  
 morphology significantly. Ghirotti et al. (2015) proposed that the land-  
 slide may have occurred when ice was still in the valley, hypothesizing  
 that the glacier could have transported a portion of the landslide  
 deposits downvalley. Thus, two hypotheses regarding the timing of the  
 landslide exist: i) the landslide occurred in the Middle Ages, long after  
 deglaciation in the area, and ii) the landslide is older, perhaps coinciding  
 with the Lateglacial period, like other rock avalanches in the region.

The landslide volume is also debated. Initially, a larger volume of  
 $20\text{--}30 \text{ Mm}^3$  concerning the whole slope was hypothesized, based on  
 geomorphological features on the Cima Salti slope (Ghirotti et al.,  
 2015). During our field survey however, only a few boulders were  
 recognised as belonging to the landslide (Fig. 4). A lithological boundary  
 between limestones of the Maiolica Formation and radiolarites of the  
 Selcifero Lombardo Formation was identified at 950–1000 m asl in the  
 depletion zone of the landslide. No radiolarite blocks were found in  
 the deposit area, suggesting the source area was much smaller than  
 originally proposed, with a volume of  $2\text{--}5 \text{ Mm}^3$ , and included only  
 Maiolica blocks. If the landslide did involve the whole slope, a significant  
 portion of the deposit is now missing. This could result from erosion and  
 transport by the Magnone stream or transport by an actively retreating  
 glacier. Neither hypothesis is satisfactory, because the erosion rate and  
 transport capacity of the stream would have had to be extremely high,

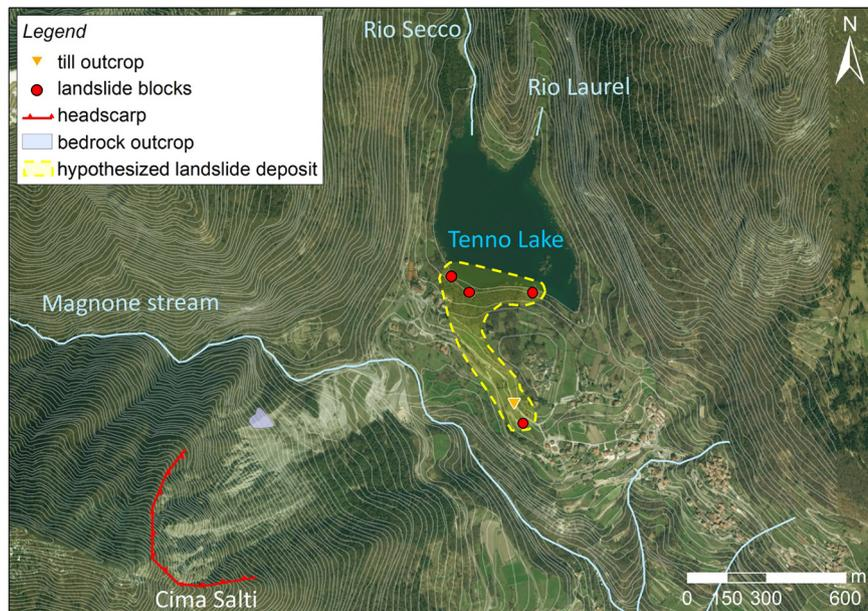


**Fig. 4.** Orthophoto of the study area; red points represent the rock blocks identified as belonging to Cima Salti landslide deposit. An interpretation of the current landslide deposit boundary is shown in yellow. Light blue curves represent local streams. (For interpretation of the references to colour in this figure legend, the reader is referred to the web version of this article.)

175 and no landslide deposits have been found downstream (Picotti, 2003;  
176 Ghirelli et al., 2015).

## 177 2. Methodology and model validation

178 This paper focuses on the use of runout modeling to understand  
179 landslide dynamics and valley evolution, and tests the two hypotheses  
180 mentioned above (Lateglacial vs. Middle Ages event). Landslide simu-  
181 lation is a good tool to confirm or question emplacement processes  
182 inferred from geological observations. As an example, such granular  
183 flow simulations of landslide runout were performed in Brunet et al.  
184 (2017) to investigate the size of individual past debris avalanches in  
185 Martinique, Lesser Antilles. Results supported field observations sug-  
186 gesting that these debris avalanches were much smaller than previously  
187 thought.

188 Granular flow models on real topography are currently used to  
189 simulate natural landslides. They are generally based on the thin-layer  
190 depth-averaging of the mass and momentum conservation equations,  
191 assuming a relatively small thickness of the fluid compared to its other  
192 dimensions, and include different friction laws. We decided here to per-  
193 form simulations using two codes, namely DAN3D and SHALTOP, widely  
194 used and validated on laboratory experiments and past landslide studies.  
195 The use of two codes may strengthen event reconstruction if the results  
196 are comparable in terms of chronologies and extents. The difference be-  
197 tween the two codes is mainly related to the description of the topogra-  
198 phy in the thin-layer approximation (i.e., shallow-water approximation)  
199 and to the numerical method used. They are both based on the descrip-  
200 tion of the granular mass as an incompressible equivalent fluid. SHALTOP,  
201 however, assumes a homogeneous and continuous material, and DAN3D  
202 discretizes the material into smooth fictitious particles, based on smoothed  
203 particle hydrodynamics (SPH). Both are very simple approaches, compared  
204 to the complexity of natural granular flows (different particle sizes, nature  
205 and shape, presence of a fluid phase, erosion processes, fragmentation, etc.)  
206 (see e.g. Delannay et al., 2017 for a review on laboratory and natural granular  
207 flows). DAN3D (McDougall and Hungr, 2004) is based on a Lagrangian  
208 numerical method, whereas SHALTOP is based on the finite volume Eulerian  
209 method (Bouchut et al., 2003; Bouchut and Westdickenberg, 2004; Mangeney-  
210 Castelnau et al., 2005; Mangeney et al., 2007). In DAN3D the user can  
211 choose among several rheologies, whereas in SHALTOP only Coulomb-type

frictions are implemented at present. Beyond the numerical method 213  
used, the originality of SHALTOP is the precise description of the topogra- 214  
phy by including in the equations the full terrain curvature tensor 215  
(Mangeney et al., 2007; Favreau et al., 2010). 216

### 217 2.1. DAN3D

Different case studies, analyzed with the codes DAN W (2D simula- 218  
tions) and DAN3D (3D simulations), and reported by several authors 219  
(Hungr and Evans, 1996; Sosio et al., 2008; Welkner et al., 2010; Sosio 220  
et al., 2012; Delaney and Evans, 2014; Schleier et al., 2015), were exam- 221  
ined to validate our models. Hungr and Evans (1996) back-analyzed 23  
rock avalanches using DAN W, changing the basal rheology from 223  
Frictional (Eq. (1)) to Voellmy (Eq. (2)) and Bingham. They concluded 224  
that, generally, the Voellmy rheology produces the best-fit results for 225  
rock avalanches, as also suggested in Pirulli and Mangeney (2008) 226  
using the code RASH3D, similar to SHALTOP (Pirulli et al., 2007). 227

$$\tau_{zx} = -\sigma_z \tan\varphi_b \quad (1) \quad 229$$

$$\tau_{zx} = -\left(\sigma_z f + \frac{\rho g v_x^2}{\xi}\right), \quad (2) \quad 230$$

where  $\tau_{zx}$  is the basal shear stress,  $\sigma_z$  is the bed-normal stress at the base 232  
of the sliding mass,  $\varphi_b$  is the bulk basal friction angle,  $f$  is the Voellmy  
friction coefficient,  $\rho$  is material density, and  $\xi$  is the Voellmy turbulence 233  
coefficient. 234

Assigning a fixed Voellmy rheology, with a 0.1 friction coefficient 235  
and a 500 m/s<sup>2</sup> turbulence coefficient, 16 of 23 cases resulted in a 236  
prediction that was within 10% of the actual runout. In two events the 237  
runout was underestimated, possibly because of fluid entrainment, 238  
whereas in five it was overestimated, possibly because no saturated 239  
soils occurred in the flow path. In Sosio et al. (2008), the runout of the 240  
Thurbieser rock avalanche (Fahrböschung = 21°, Italian Central Alps) 241  
was simulated. Results were constrained using the final geometry, 242  
characteristics of the deposit and the mean front velocity, estimated 243  
from videos taken during the phenomenon. A Frictional rheology was 244  
implemented on the failure surface and on rock outcrops, whereas a 245  
Voellmy rheology was assumed for glacial ice. The values of the adopted 246  
parameters are reported in Table 1. In the same work, typical ranges of 247

t1.1 **Table 1**  
t Q2 Back-calculated values for the rock avalanches analyzed in literature using DAN3D.

t1.3	Reference	Event	Material	Rheology	$\Phi_b$ (°)	$\mu$	$\xi$ (m/s <sup>2</sup> )	H/L	Volume (Mm <sup>3</sup> )	
t1.4	Hungre and Evans (1996)	Various	–	Frictional	8–23	–	–	–	–	
t1.5				Voellmy	–	0.03–0.24	–	100–1000	–	–
t1.6	Sosio et al. (2008)	Thurwieser	Source	Frictional	24	–	–	0.48	2.5	
t1.7				Frictional	26	–	–	–	–	–
t1.8				Voellmy	–	0.05	1000	–	–	–
t1.9				Frictional	26	–	–	–	–	–
t1.10	Welkner et al. (2010)	Portillo	Source	Frictional	30	–	–	–	50	
t1.11				Voellmy	–	0.1	500	–	(2 events)	
t1.12	Sosio et al. (2012)	Various	–	Frictional	2.75–26	–	–	0.11–0.48	1–20	
t1.13				Voellmy	–	0.03–0.1	1000–2000	–	–	
t Q3				Voellmy	–	0.08	1050	0.185	3.2	
t1.15	Schleier et al. (2015)	Innerdalen	Snow-covered glacier	Voellmy	–	0.15	500	0.23–0.42	23.5–31.5	
t1.16				Voellmy	–	0.06	1000	–	–	

248 values found in literature are reported, organized based on the analyzed  
249 phenomena and involved materials. For rock avalanches, debris  
250 avalanches and rockslides, a range of friction angles between 8° and  
251 30° was used when a Frictional rheology was chosen, whereas a friction  
252 coefficient of 0.05–0.25 (i.e. friction angles between about 3° to 14°) and  
253 a turbulence coefficient varying between 200 and 1000 m/s<sup>2</sup> were  
254 adopted using the Voellmy rheology. In Welkner et al. (2010), the  
255 results of a back analysis of the prehistoric Portillo rock avalanche in  
256 Chile were compared with the current distribution of rockslide deposits.  
257 They indicated the presence of two separate sliding events originating  
258 from different sources. A Frictional rheology was adopted in the source  
259 area, whereas a Voellmy rheology was considered in the distal part  
260 (valley floor), as this combination best fit field observations. In Sosio  
261 et al. (2012) a review of the best-documented ice-rock avalanches is  
262 presented. The authors back analyzed these events (volume ranging  
263 between 1 and 14 Mm<sup>3</sup>) using SPH and FEM numerical methods,  
264 employing Frictional and Voellmy rheologies. Generally, for the Voellmy  
265 rheology, the friction coefficient ranges between 0.03 and 0.1 and the  
266 turbulence coefficient is between 1000 m/s<sup>2</sup> and 2000 m/s<sup>2</sup>. For the  
267 Frictional rheology, the bulk friction angle is 2.75° to 26°, with values  
268 inversely related to event volumes. In Delaney and Evans (2014), a  
269 Voellmy rheology was used to simulate the 1997 Mount Munday rock  
270 avalanche (Fahrböschung = 10°, BC, Canada). The authors focused on  
271 the geometric characteristics of the debris sheet. In glacial environ-  
272 ments deposits are usually more extensive in area relative to volume  
273 than rock avalanches in non-glacial environments. In Schleier et al.  
274 (2015), DAN3D runout analyses were used to understand the origin of  
275 a rock-boulder deposit in Innerdalen, Norway. Voellmy rheology was  
276 used both for the natural slope and for the glacier surface (values are  
277 shown in Table 1).

## 278 2.2. SHALTOP

279 The SHALTOP code has been used to reproduce experimental  
280 granular flows and natural landslides. Simulations were shown to  
281 reproduce the deposit characteristics of lab-scale granular flow experi-  
282 ments well (Mangeney-Castelnau, 2005; Mangeney et al., 2007; Lucas  
283 et al., 2014). In Kuo et al. (2009), the back analyzed basal friction  
284 angle ( $\varphi = 6^\circ$ ) of the simulation of the very large Tsaoiling  
285 earthquake-triggered rock avalanche in Taiwan (volume of 126 Mm<sup>3</sup>)  
286 was found to be considerably lower than the internal peak friction  
287 angle of the Cholan Formation, comprising sandstones and intercalated  
288 shales (Table 2). Indeed, for large-volume landslides (>1 Mm<sup>3</sup>), the  
289 empirical friction angle is usually found to be smaller than the typical  
290 friction angle of the involved material (Campbell et al., 1995; Pirulli  
291 and Mangeney, 2008).

292 By analyzing and simulating tens of landslides with a wide range of  
293 volumes using SHALTOP, Lucas et al. (2014) showed that the empirical  
294 effective friction required in the model to reproduce the landslide  
295 runout decreases with the volume. They proposed an empirical fit

relating the effective Coulomb friction coefficient  $\mu = \tan \varphi$  to the 296  
volume involved V: 297

$$\mu = V^{-0.0774} \quad (3)$$

299 They found values as small as  $\mu = 0.11$  ( $\varphi = 6^\circ$ ) for volumes as large  
as 36 km<sup>3</sup>. By comparing seismic data and numerical modeling with  
SHALTOP, Levy et al. (2015) showed that this empirical volume-  
dependent friction was able to explain the seismic signal of 200 rockfalls  
in Montserrat (for volumes up to 1 Mm<sup>3</sup>), whereas a constant friction  
coefficient was not. Using seismic data makes it possible to calibrate the  
friction coefficient based on the landslide deposit and on its dynamics.  
Favreau et al. (2010) simulated the Thurwieser landslide; the model  
was calibrated using the seismic signal generated by the landslide. A  
Frictional rheology was assumed with a friction angle of 6° for the glacier  
and 26° everywhere else. These values are similar to the ones found for  
the same event using the DAN3D code by Sosio et al. (2008). Comparison  
between SHALTOP simulations and seismic signals suggested a friction  
angle of 35° for small rockfalls ( $V < 2000 \text{ m}^3$ ) in La Réunion. The 2005  
Mount Steller rock-ice avalanche in Alaska, USA was simulated in  
Moretti et al. (2012). The initial mass was composed of rock, ice, and  
snow; the path included bedrock and a glacier. In this case the frictional  
parameters were also assessed by comparing the simulation results  
with the seismic signal recorded by 7 broadband seismic stations. The  
Mount Meager landslide (6 August 2010, BC, Canada), which initiated as  
a rockslide and rapidly transformed into a debris flow, was simulated by  
Moretti et al. (2015). They assumed different friction coefficients for the  
parts of the path where the rockslide travelled and where the event  
evolved into a debris flow. They assigned a lower friction angle to the gla-  
cier. The calibrated values of the friction coefficient on the glacier are in  
the same range for these different case studies (friction angles 5–7°).  
Yamada et al. (2016, 2018) simulated four landslides in Japan with vol-  
umes of 2–8 Mm<sup>3</sup>. Friction coefficients between 0.3 and 0.4 (i.e. friction  
angles 16.7°–21.8°) were constrained from comparison with seismic  
data, in good agreement with Lucas et al. (2014) (i. e. Eq. (3)).

Because of the lack of field evidence at Cima Salto (uncertain deposit  
thickness, landslide velocities, deposit shape and location), the most  
widely used rheological relationships and a range of model parameters  
were initially chosen from the back analyses of similar case studies de-  
scribed in literature. For our models, we used the parameters reported  
in Table 3 for rock and ice materials, based on the rock mass and runout  
characteristics observed in the field and the values found in literature  
(Tables 1 and 2). In DAN3D, the unit weights of rock mass and ice were  
kept constant at 20 kN/m<sup>3</sup> and 9 kN/m<sup>3</sup>, respectively. The internal fric-  
tion angle (varying from 30° to 35° for rock and held constant at 40°  
for ice, based on values from the literature) did not have a significant  
effect on the results, and, hence, these are not presented in this paper.  
The number of smooth particles was set to 4000 (maximum number of  
particles). In the absence of more detailed information, the rate of ero-  
sion was set to zero, i.e. entrainment was neglected. Other parameters

**Table 2**  
Back-calculated values for the rock avalanches analyzed in the literature using SHALTOP.

Reference	Event	Material	Rheology	$\varphi_b$ (°)	H/L	Volume (Mm <sup>3</sup> )
Kuo et al. (2009)	Tsaoling	Natural slope	Frictional	6	0.3125	126
Favreau et al. (2010)	Thurwieser	Natural slope	Frictional	26	0.48	2.5
		Glacier	Frictional	6		
Hibert et al. (2011)	La Réunion rockfalls	Natural slope	Frictional	35	–	(1–2000 m <sup>3</sup> )
Moretti et al. (2012)	Mount Steller	Natural slope	Frictional	11–18	–	40–60
		Glacier	Frictional	7		
Lucas et al. (2014)	Various	–	Frictional	6–35	–	–
Moretti et al. (2015)	Mount Meager	Natural slope (rockslide)	Frictional	18	–	48.5
		Natural slope (debris flows)	Frictional	8		
		Glacier	Frictional	5		
Levy et al. (2015)	Montserrat rockfalls, pyroclastic flows	Natural slope	Frictional	19–31.7		(500–10 <sup>6</sup> m <sup>3</sup> )
Yamada et al. (2016)	Akatani	Natural slope	Frictional	16.7	–	8.2
Yamada et al. (2018)	Iya	Natural slope	Frictional	17.7		4.67
Yamada et al. (2018)	Nagatono	Natural slope	Frictional	21.8		3.63
Yamada et al. (2018)	Nono	Natural slope	Frictional	19.8		2.72

and options were set based on the suggestions given in literature and in the software manual. For SHALTOP, we used the Coulomb frictional model, and the same material parameters as the DAN3D Frictional simulations. A downsampled DEM with a pixel resolution of 40 × 40 m was used for both programs; this resolution was considered adequate given the uncertainties in the paleo-topography and the benefit of reduction in simulation time. The topography of the area was derived from the 1983 contour lines, i.e. before the remobilization of the lower portion of the slope and associated stabilization works in 2000. Two scenarios were created to simulate the landslide in the Middle Ages (after Alessio et al., 1973) and in the Lateglacial period (Fig. 5). In the first case, the valley topography was modified by decreasing the depth of incision of the Magnone stream. For the Lateglacial simulations a reconstruction of the glacier occupying the Magnone valley was attempted. Field evidence of kame terraces and the reconstruction of the glacier in the neighbouring Ledro valley (Picotti, 2003) were used. Two different landslide volumes were hypothesized from the 3D reconstruction of the original topography, based on similar slopes in the surrounding area. Assuming a failure of the whole slope, a volume of about 18 Mm<sup>3</sup> was found, whereas limiting the failed area to the upper portion of the Cima Salti slope, i.e. including only the Maiolica Formation, produced an estimated volume of 2.2 Mm<sup>3</sup>.

Based on these input data, several simulations were conducted using the two numerical codes, varying material properties systematically. DAN3D simulations were completed first, and then compared with SHALTOP simulations. The analysis results, considering deposit location and thickness, were then compared with the available field data to constrain the simulations and discriminate between more and less plausible hypotheses. Based on field investigations and literature (Picotti, 2003):

- the geomorphology of the investigated area was not significantly influenced by the landslide, suggesting a small thickness of the landslide deposit;
- no deposits were found downstream along the Magnone river;
- the position of the blocks belonging to the landslide deposit and the lack of deposits in other areas were used to constrain the simulation results (Fig. 4).

**Table 3**  
Values adopted in the DAN3D and SHALTOP simulations.

Scenario	Material	Rheology	$\Phi_b$ (°)	$\mu$	$\xi$ (m/s <sup>2</sup> )
Without glacier	Rock outcrops	Frictional	5–35	–	–
		Voellmy	–	0.03–0.25	250–2000
With glacier	Rock outcrops	Frictional	5–35	–	–
		Voellmy	–	0.03–0.25	250–2000
	Glacier	Frictional	4–6	–	–
		Voellmy	–	0.05–0.15	1000–2000

Particular attention was paid to analyzing the results in which the landslide deposit could have dammed the river and, thus, created Tenno Lake.

Below, we investigate whether: i) the Cima Salti Landslide involved a large (18 Mm<sup>3</sup>) or small (2.2 Mm<sup>3</sup>) volume, and ii) the Cima Salti Landslide occurred in an ice-free valley or when glacial ice was still present at the base of the slope.

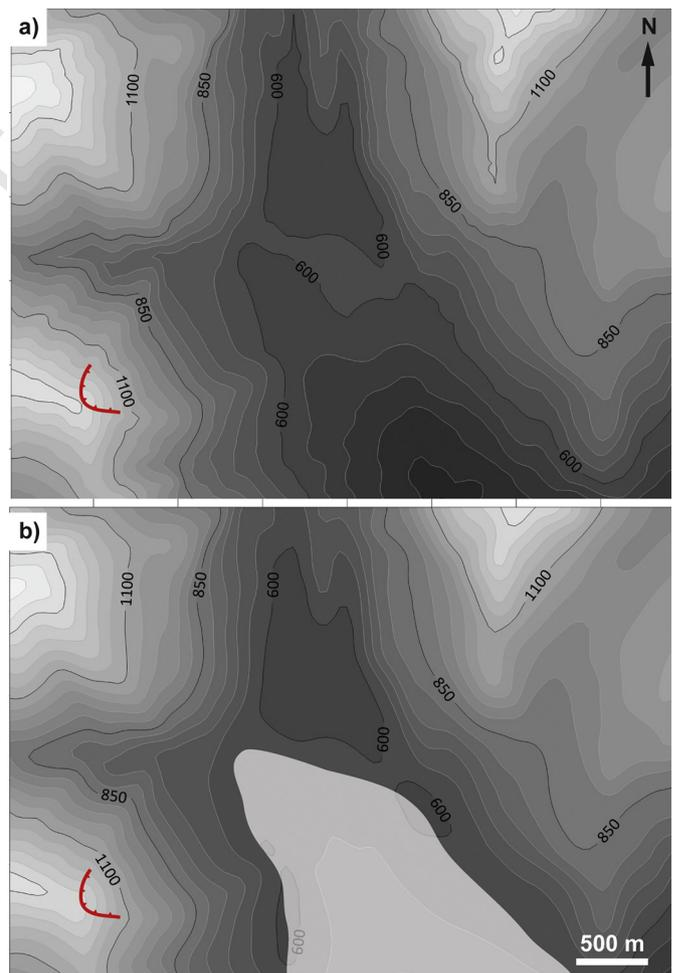


**Fig. 5.** Input topographies for scenarios without glacial ice (a) and with glacial ice (b). The red curve represents the headscarp of the Cima Salti Landslide, and the grey area in (b) is the ice. Compare with Fig. 4 for present-day topography. Contour intervals = 25 m. (For interpretation of the references to colour in this figure legend, the reader is referred to the web version of this article.)

### 388 3. How large was the Tenno Landslide?

389 Considering the large (18 Mm<sup>3</sup>) landslide volume, none of the sim-  
 390 ulations performed using the Voellmy rheology lead to a landslide  
 391 dammed lake. Using a low value of  $\mu$  (<0.15) or a very high value of  $\xi$   
 392 (1000 m/s<sup>2</sup>), part of the landslide material stopped in the lake depres-  
 393 sion and part travelled downstream. With higher values of  $\mu$  (>0.15)  
 394 most of the deposit was found at the foot of the slope (Fig. 6).

395 In the large volume Frictional rheology models, simulations with a  
 396 basal friction angle higher than 15° showed that the landslide material  
 397 came to rest at the foot of the slope. Note that this friction angle  
 398 corresponds to the value obtained with the empirical friction law in  
 399 Eqs. (1) and (3) for a volume of 18 Mm<sup>3</sup> (15.3°), whereas this law gives  
 400 a friction angle of 17.9° for  $V = 2.2$  Mm<sup>3</sup>. When the basal friction angle  
 401 was decreased to 10°, which is small for this volume according to  
 402 Eq. (3), the landslide material spread into the middle of the valley, with  
 403 a maximum thickness of approximately 30 m at the base of the Cima  
 404 Salti slope and about 6.5 m in the SW portion of the current Tenno Lake  
 405 (Fig. 7). With an average lake depth of about 20 m, this deposit thick-  
 406 ness would probably not have been enough to dam the river for a long period  
 407 of time and create Tenno Lake. Furthermore, the lake would probably  
 408 have had a different shape. With lower friction angles the landslide materi-  
 409 al mainly accumulated in the lake depression or moved downstream.

410 With the smaller volume, changing the parameters of the Voellmy  
 411 rheology in the defined range of values, two typical scenarios were  
 412 identified:

- 413 - with low values of  $\mu$ : most of the landslide deposit travelled down-  
 414 stream; in several cases (with higher values of  $\xi$ ) part of the deposit  
 415 entered the depression in the middle of the valley;
- 416 - with high values of  $\mu$  (>0.1): the landslide material was deposited at  
 417 the foot of the Cima Salti slope, not reaching the middle of the valley  
 418 (Fig. 8).

420 Using the Frictional rheology, with lower values of the basal friction  
 421 angle (5 and 10°), the landslide material was deposited partly in the  
 422 lake depression and partly on the sides of the valley (Fig. 9), without

423 creating the condition for a possible river damming, i.e. the deposit  
 424 was too spread out and did not completely block the valley bottom.  
 425 The distributions did not coincide with the location of the deposits  
 426 mapped in the field.

427 With a basal friction angle of 15° the landslide deposit is located in  
 428 the middle of the valley (Fig. 10). The maximum thickness of the deposit  
 429 reaches 13 m in the region just below the Cima Salti slope and 1.5 m in  
 430 the SW part of the current Tenno Lake. According to these results, the  
 431 shape of the deposit and its thickness would probably not have been  
 432 sufficient to dam the river and create Tenno Lake. In this simulation  
 433 and the one illustrated in Fig. 7 (larger volume, Frictional rheology  
 434 with a basal friction angle of 10°), however, material accumulates in  
 435 the area where a little island is located, in the SE part of the lake.  
 436 Comparing these two simulations with the landslide blocks mapped in  
 437 the area some discrepancies were found in the eastern part of the valley,  
 438 where deposit locations in both simulations do not correspond to field  
 439 observations. Moreover, in these two simulations, part of the landslide  
 440 material travelled downstream, where no evidence was found in the  
 441 field (Picotti, 2003; Ghirotti et al., 2015).

442 When the basal friction angle was changed to 17–18°, the area occu-  
 443 pied by the landslide deposit was very similar to the one derived from  
 444 field evidence. This value of the friction angle coincides with that of  
 445 17.9° given by Eq. (3). The thickness, position and shape of the deposit  
 446 were probably not compatible with long-term damming of the river.  
 447 For example, water would be able to flow around the proximal and distal  
 448 margins of the deposits. No stratigraphic evidence or strand lines  
 449 have been found to suggest long-standing water or outburst floods.

450 In all small-volume simulations, the resulting maximum deposit  
 451 thickness is quite small, typically around 10 m, except for the simula-  
 452 tions with higher friction angles (20–35°), whereas in the simulations  
 453 performed using a larger volume the maximum deposit thickness is al-  
 454 ways larger than 20 m, reaching values of 65 m with the higher friction  
 455 angles (Fig. 11). Since significant changes in the valley geomorphology  
 456 because of the Cima Salti Landslide are not expected, very thick deposits  
 457 were not considered as plausible.

458 The landslide reached a velocity peak approximately 20 s after initi-  
 459 ation (Fig. 12) in the DAN3D simulations; the main event had a duration

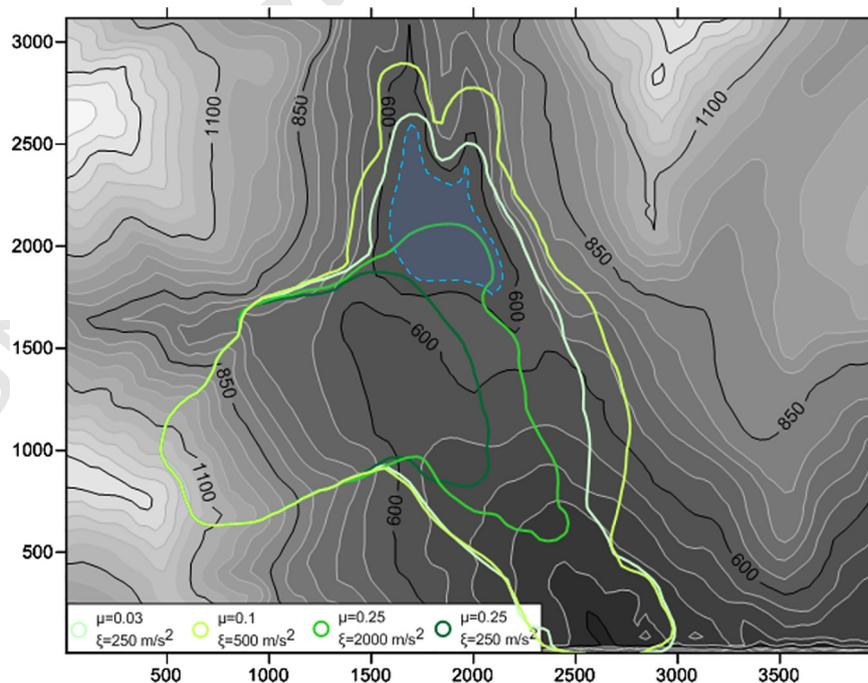


**Fig. 6.** The effect of friction and turbulence parameters on impact area for DAN3D Voellmy rheology ice-free simulations with larger volume (18 Mm<sup>3</sup>). Note that the green outlines are the maximum thickness = 2 m contours. Blue area represents current extent of Tenno Lake for reference. Relative north and east scales (starting at 0 in the bottom left corner) are in metres. (For interpretation of the references to colour in this figure legend, the reader is referred to the web version of this article.)

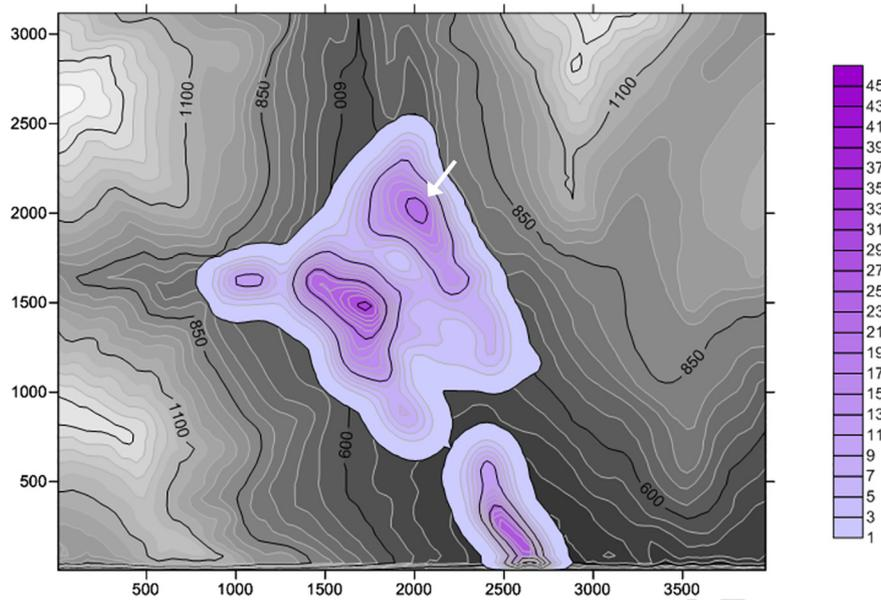


**Fig. 7.** Final results of the DAN3D simulation, deposit thickness (contours in metres, see colour bar). Simulation with larger volume ( $18 \text{ Mm}^3$ ), frictional rheology, basal friction angle  $10^\circ$ . White arrow indicates location of island. Relative north and east scales (starting at 0 in the bottom left corner) are in metres.

460 of  $<70$  s. SHALTOP and DAN3D models with Frictional rheology showed  
 461 similar responses (Figs. 12 and 13). In the SHALTOP simulation, the  
 462 landslide reached the bottom of the valley between 40 s and 60 s after  
 463 the failure initiation, then, approximately 20 s later, the material started  
 464 to run up the topographic high in the middle of the valley and finally  
 465 came to a halt. The main movement phase lasted  $<80$  s, whereas the  
 466 entire event had a duration of  $<100$  s. The duration of the event is similar  
 467 in the two codes. Generally, the SHALTOP simulations seemed to  
 468 be more affected by the topographic roughness and showed slightly  
 469 more distributed deposits. With higher values ( $20\text{--}35^\circ$ ) the landslide  
 470 material stopped at the foot or even in the middle part of the slope  
 471 (Fig. 9).

#### 4. What was the role of ice at Tenno?

472

The results of the simulations with glacial ice in the Magnone valley  
 473 bottom are highly dependent on the ice location and morphology. Using  
 474 an ice friction angle of  $4^\circ$ , the DAN3D Frictional rheology simulations  
 475 run with low to intermediate basal friction angles show the deposits  
 476 of even the small unstable volume reaching the opposite valley flank  
 477 (Fig. 14). Only with sliding mass friction angles above  $20^\circ$  do most of  
 478 the deposits come to rest at the base of the source area. With basal  
 479 friction angles  $\leq 20^\circ$  most of the deposits travel across the glacier tongue  
 480 into the depression of Tenno Lake, with maximum deposit depths of  
 481  $<20$  m. With a friction angle of  $17^\circ$  (based on deposit distribution  
 482

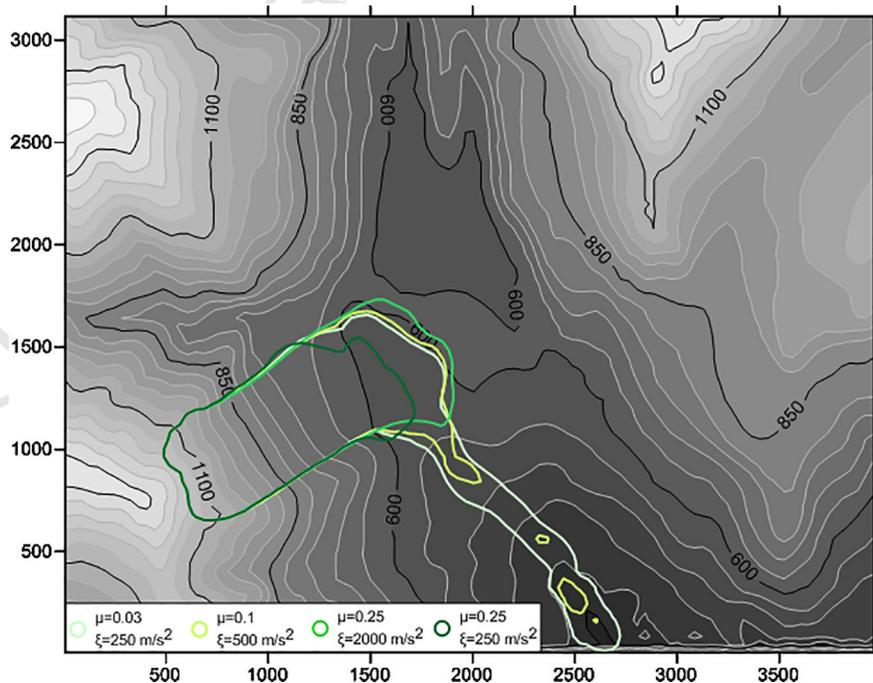


**Fig. 8.** Impact areas for some of the DAN3D Voellmy rheology, smaller volume ( $2.2 \text{ Mm}^3$ ). Note that the green outlines are the maximum thickness = 2 m contours. Relative north and east scales (starting at 0 in the bottom left corner) are in metres. (For interpretation of the references to colour in this figure legend, the reader is referred to the web version of this article.)

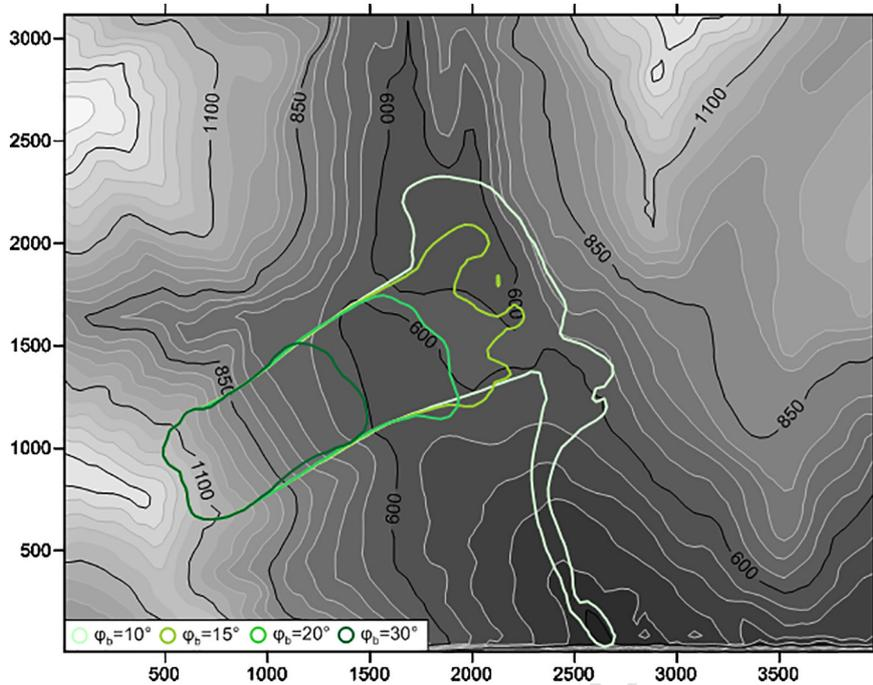


**Fig. 9.** The effect of friction angle on impact area for the DAN3D Frictional rheology, smaller volume ( $2.2 \text{ Mm}^3$ ). Note that the green outlines are the maximum thickness = 2 m contours. Relative north and east scales (starting at 0 in the bottom left corner) are in metres. (For interpretation of the references to colour in this figure legend, the reader is referred to the web version of this article.)

483 observed in the field, the most likely simulations correspond to friction  
484 angle values between  $15^\circ$  and  $20^\circ$ , as in the ice-free simulations), the  
485 maximum deposit depth is located where the island in Tenno Lake is  
486 currently situated (Fig. 15).

487 The simulations with the large volume show similar distributions of  
488 deposits, but deposit thickness reaches 45 m. Again, basal friction angles  
489 of  $>20^\circ$  resulted in the deposits coming to rest at the base of the Cima  
490 Salti slope.

491 The DAN3D Frictional and SHALTOP results are comparable, particu-  
492 larly when considering deposit thicknesses  $> 5 \text{ m}$  (Fig. 15). Both show  
493 deposits east and west of the glacier ice in the valley bottom; however,

SHALTOP also shows deposits on the slope south of the landslide  
494 headscarp and in the upper reach of the Magnone streambed. Most  
495 SHALTOP simulations assumed an ice friction angle of  $4^\circ$ . The results of  
496 those with a  $6^\circ$  ice friction angle did not differ significantly from the  $4^\circ$   
497 simulations. For example, with a rock basal friction angle of  $17^\circ$ ,  
498 maximum deposit thickness decreased slightly (from 22 to 20 m), and  
499 runout increased by a few metres relative to the  $4^\circ$  simulations. 500

The friction coefficient dominated runout response in the DAN3D  
501 Voellmy simulations. When  $\mu > 0.2$ , the deposits came to rest at the  
502 base of the slope. With lower friction coefficients ( $\mu \leq 0.1$ ), the deposits  
503 travelled across the valley. With a constant friction coefficient (for  
504

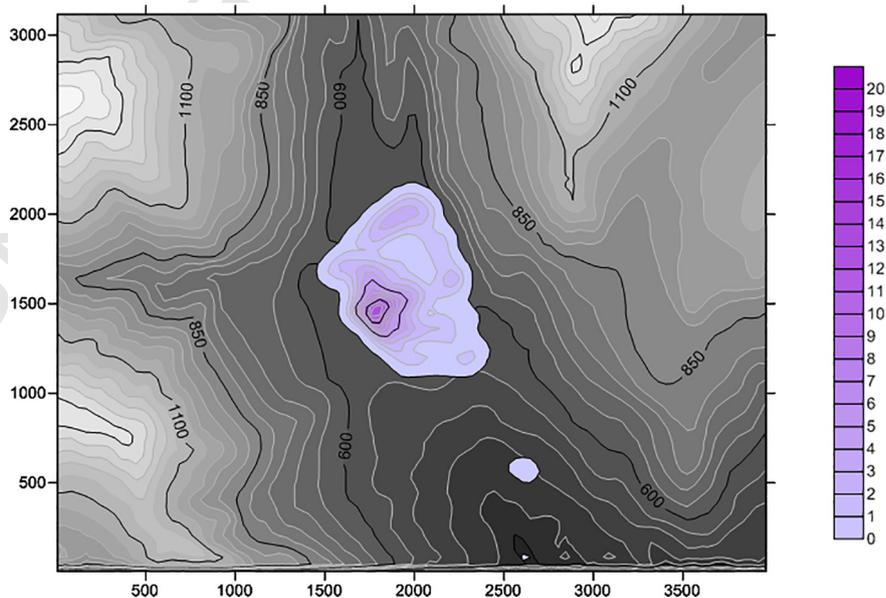


**Fig. 10.** Deposit thickness results (contours in metres, see colour bar) of the DAN3D simulation with smaller volume ( $2.2 \text{ Mm}^3$ ), Frictional rheology, basal friction angle  $15^\circ$ . Relative north and east scales (starting at 0 in the bottom left corner) are in metres. (For interpretation of the references to colour in this figure legend, the reader is referred to the web version of this article.)

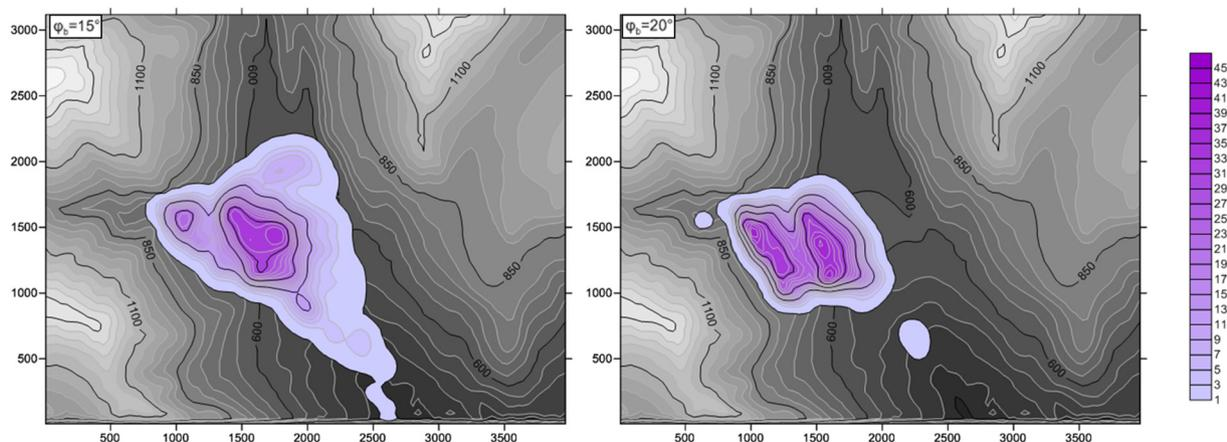


**Fig. 11.** Final results of the DAN3D simulation, deposit thickness (contours in metres, see colour bar). Simulation with larger volume ( $18 \text{ Mm}^3$ ), frictional rheology, basal friction angle  $10^\circ$  (on the left) and  $20^\circ$  (on the right). Relative north and east scales (starting at 0 in the bottom left corner) are in metres. (For interpretation of the references to colour in this figure legend, the reader is referred to the web version of this article.)

505 example,  $\mu = 0.03$  in Fig. 16), a high turbulence coefficient corresponded  
 506 with a longer runout. Low values resulted in proportionally more deposits  
 507 travelling down the west side of the Magnone valley between the valley  
 508 flank and ice, whereas high values caused proportionally more of the  
 509 deposits to cross the ice and valley to the NE. The Voellmy simulations  
 510 showed distinct deposit thickness distributions when compared to both  
 511 the DAN3D Frictional and SHALTOP results, and the deposits commonly  
 512 separated into two main clusters, one in the lake and the other along  
 513 the base of Cima Salti. These deposit distributions correlate poorly with  
 514 our field observations.

515 When the source area was classified as having a Frictional rheology  
 516 ( $\varphi_b = 17^\circ$ ), and the ice as Voellmy ( $\mu = 0.05$ ,  $\xi = 1000 \text{ m/s}^2$ ) as in  
 517 Sosio et al. (2008), the centre-of-mass of the deposits travelled farther  
 518 than in the Frictional ice simulations, across the glacier tongue. The  
 519 deposits were also more distributed, coming to rest around the glacier  
 520 tongue rather than on the ice.

521 The maximum model velocity of reasonable simulations did not ex-  
 522 ceed  $70 \text{ m/s}$ . The maximum model velocity reached in the most realistic  
 523 simulation ( $\varphi_b = 17^\circ$ ) was  $69 \text{ m/s}$ , comparable to the ice-free simulations  
 524 above, whereas the average velocity was significantly lower ( $<30 \text{ m/s}$ )  
 525 (Fig. 17). The duration of the main event, approximately  $70\text{--}80 \text{ s}$ , was  
 526 similar to the ice-free simulations. The durations of the main movements  
 527 (i.e., not reactivations of parts of the sliding mass after most of the deposit  
 528 has come to rest) of the larger volume ( $18 \text{ Mm}^3$ ) models increased to

$100\text{--}200 \text{ s}$ , with residual movements of up to  $10 \text{ m/s}$  lasting up to  $529$   
 $5000 \text{ s}$  ( $83 \text{ min}$ ). 530

## 5. Discussion and conclusions 531

The results of the DAN3D and SHALTOP simulations provide valuable 532  
 insight into the Cima Salti Landslide. The DAN3D Frictional rheology 533  
 produced more reasonable results than the Voellmy simulations, and 534  
 compared well with the results of the SHALTOP model, validating the 535  
 use of both codes. For example, in the most likely scenario (i.e., glacial 536  
 ice with  $\varphi = 4^\circ$ , Frictional rheology,  $\varphi = 17^\circ$ ), the two codes show a 537  
 difference of approximately  $36\%$  in the deposit area (DAN3D deposit is 538  
 larger) and roughly  $6\%$  difference considering the duration of the 539  
 event (the DAN3D main event lasts  $85 \text{ s}$  and SHALTOP  $90 \text{ s}$ ). Based on 540  
 the lithology and the limited distribution and thickness of landslide 541  
 blocks found in the field, the small volume simulations seem to be 542  
 more realistic. If the Cima Salti Landslide involved the entire slope, a 543  
 large portion of the deposits is now missing. 544

The ice-free and glacier Frictional models indicate that the most rea- 545  
 sonable basal friction value is  $17^\circ\text{--}20^\circ$ , based on deposit runout and 546  
 thickness, and field investigations. This agrees well with Hungr and 547  
 Evans (1996), Moretti et al. (2012) and the empirical friction law 548  
 (Eq. (3)) of Lucas et al. (2014) (Fig. 18). This is, however, lower than 549  
 the friction angle found in Favreau et al. (2010) for the Thurwieser 550

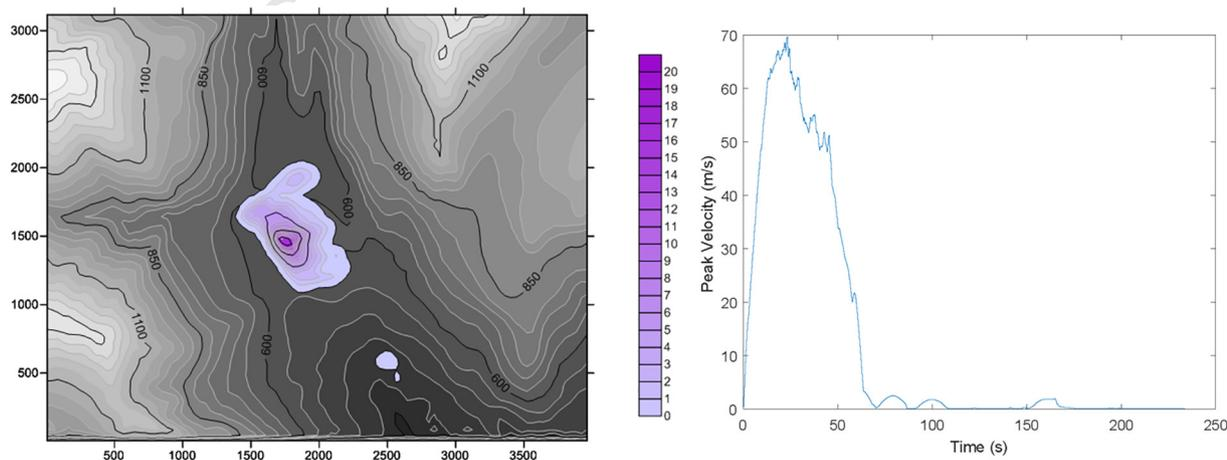


**Fig. 12.** Final results of the DAN3D simulation, deposit thickness (contours in metres, see colour bar). Relative north and east scales (starting at 0 in the bottom left corner) in left figure are in metres. Simulation with smaller volume ( $2.2 \text{ Mm}^3$ ), Frictional rheology, basal friction angle  $17^\circ$ . (For interpretation of the references to colour in this figure legend, the reader is referred to the web version of this article.)

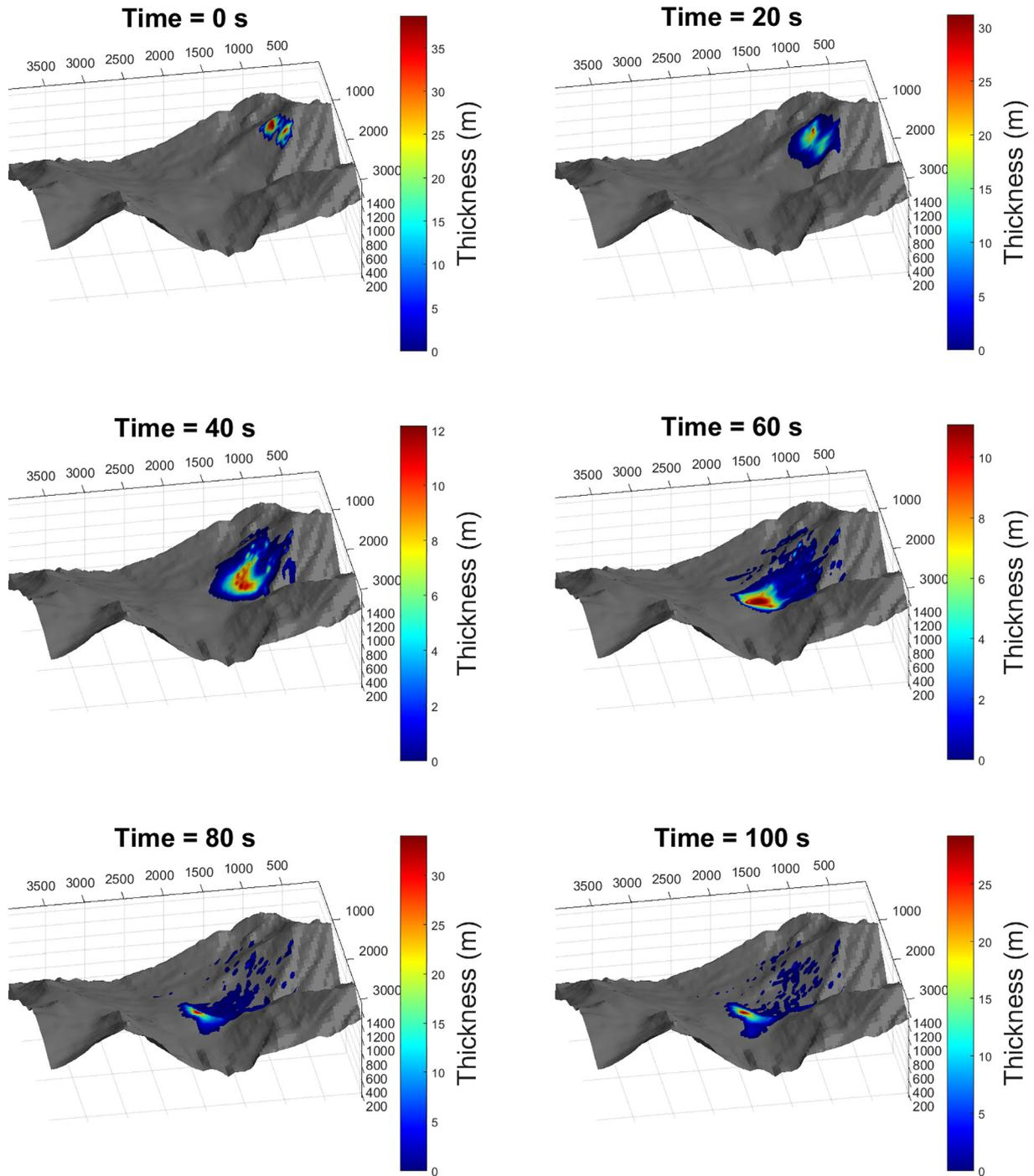
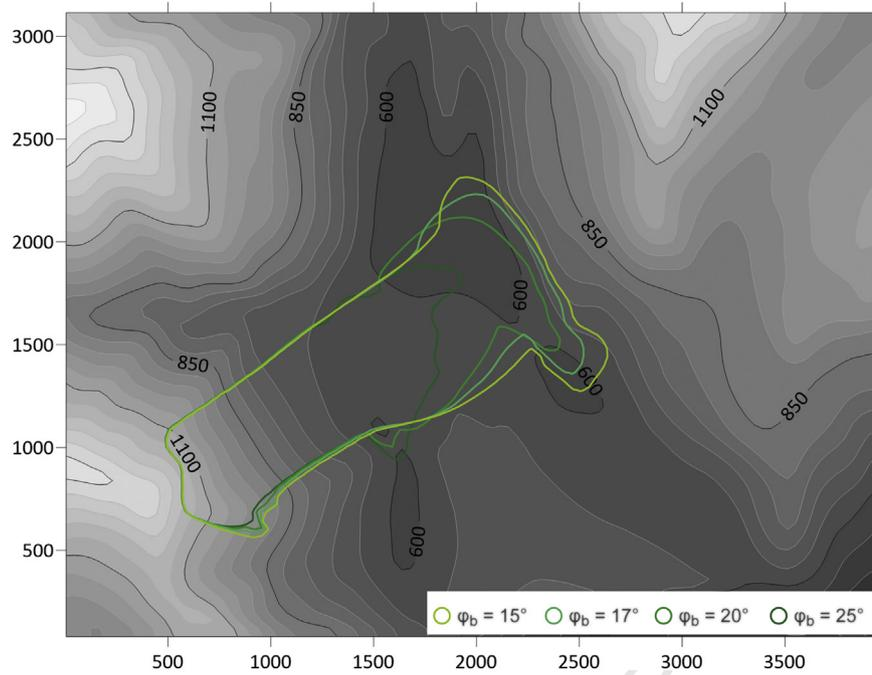


Fig. 13. Results of the SHALTOP simulation at different times. Simulation with smaller volume ( $2.2 \text{ Mm}^3$ ), Frictional rheology, basal friction angle  $17^\circ$ .

551 landslide with a similar volume. The simulated failures attain maximum  
 552 velocities of 70 m/s, and durations of approximately 70–80 s, indicating  
 553 the landslide failed as a rapid rock avalanche.

554 The obtained results were compared with the rheology parameters  
 555 reported in literature. The Eperon de la Brenva, Martin River Unnamed 1  
 556 and Becca di Luseny ice-rock avalanches (Sosio et al., 2012) have sim-  
 557 ilar volumes ( $1.1\text{--}4.4 \text{ Mm}^3$ ) and H/L values (0.39–0.42) to the Cima Salti  
 558 Landslide. In these cases, the friction angle used for the simulations is  
 559 lower ( $\varphi_b = 9\text{--}12^\circ$ ) than the one obtained for Cima Salti. This could re-  
 560 sult from the large entrainment of ice and snow, which resulted in a low  
 561 shear resistance and longer runout distances (see e.g. Mangeney et al.,  
 562 2010 and Farin et al., 2014 for increase in runout distance in granular

563 flows on erodible beds). Evans et al. (2001) simulated the 1984 Turbid 563  
 564 Creek rock avalanche (volume =  $0.74 \text{ Mm}^3$ ,  $\varphi = 19^\circ$ ). They proposed 564  
 565 a Voellmy and a Frictional rheology ( $\varphi_b = 30^\circ$ ), even if the simulated 565  
 566 velocities appeared to be too high in the Frictional rheology simulations. 566  
 567 The Thurwieser rock avalanche was found to be very similar to the Cima 567  
 568 Salti Landslide (Fig. 19). It is one of the few events recorded on video, 568  
 569 and, thus, its exact duration, velocities, source area, travel paths, and 569  
 570 deposition location are known. Furthermore, it was simulated with 570  
 571 DAN3D and SHALTOP (Sosio et al., 2008; Favreau et al., 2010). In the 571  
 572 DAN3D models, the best simulation was obtained with a Frictional 572  
 573 rheology ( $\varphi_b = 24\text{--}26^\circ$ ) for the rock outcrops and a Voellmy rheology 573  
 574 for the glacier ( $\mu = 0.05$ ,  $\xi = 1000 \text{ m/s}^2$ ). Using SHALTOP, almost the 574



**Fig. 14.** The effect of basal friction angle on impact area for the DAN3D Frictional rheology glacial ice simulations with small volume ( $2.2 \text{ Mm}^3$ ). Note that the green outlines are the maximum thickness = 2 m contours. Relative north and east scales (starting at 0 in the bottom left corner) are in metres. (For interpretation of the references to colour in this figure legend, the reader is referred to the web version of this article.)

575 same parameters were used for the rock outcrops, whereas a friction  
576 angle of  $6^\circ$  was used for the glacier. The duration and velocities mea-  
577 sured for the Thurwieser rock avalanche (duration of 75–90s, mean ve-  
578 locity of 36–38 m/s, highest values of 60–65 m/s) are comparable to the  
579 ones obtained from the simulations of the Cima Salti Landslide.

580 All simulations indicated a travel path previously not considered for  
581 the Cima Salti Landslide. The headscarp crosses the south ridge on Cima  
582 Salti, and, thus, a minor secondary component of the slide could have  
583 travelled into the adjacent watershed. Certainly, mass movement  
584 material is found in this watershed, but its origins are unknown.

585 Given the extensive distribution of till in the area and the lack of  
586 landslide debris, it seems likely that the Cima Salti Landslide deposited  
587 material on ice. Had the landslide occurred in the Middle Ages, the  
588 deposits would have been more widespread today, as the Magnone  
589 stream could not have removed as much material as suggested by the  
590 current distribution of landslide debris.

591 The tree dates cited in previous papers are also questionable. The me-  
592 dieval age of the landslide is based on radiocarbon dating of fossil trunks  
593 found underwater dated to 1040–1215 CE (Alessio et al., 1973). This  
594 agrees well with the age of forests that occupied former lake shores

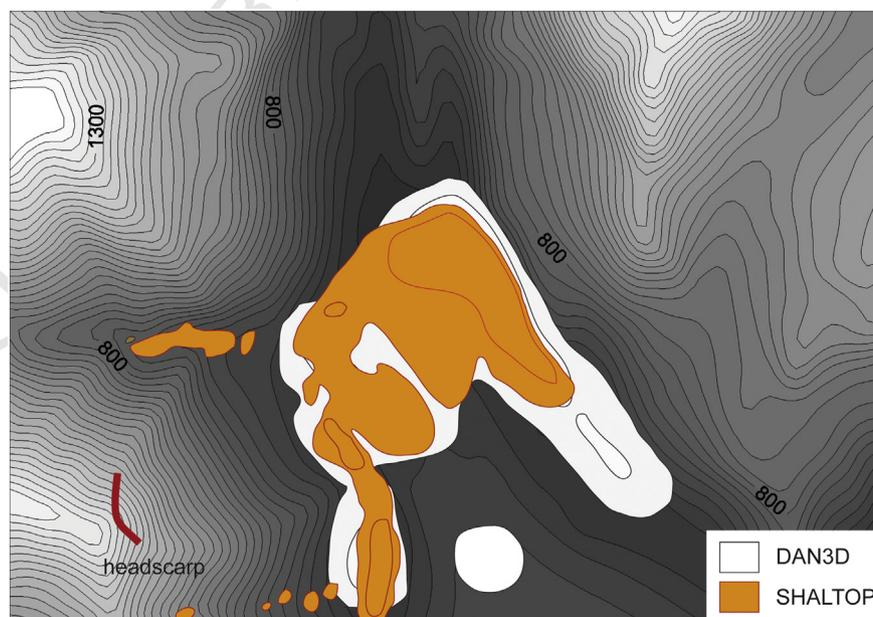


**Fig. 15.** Comparison of the DAN3D and SHALTOP thickness results at the end of simulation time (velocity  $\approx 0 \text{ m/s}$ ) for a basal friction angle of  $17^\circ$  (rock) and  $4^\circ$  (ice), small volume ( $2.2 \text{ Mm}^3$ ). Only the 0 and 5 m thickness contours are shown. Relative north and east scales (starting at 0 in the bottom left corner) are in metres.

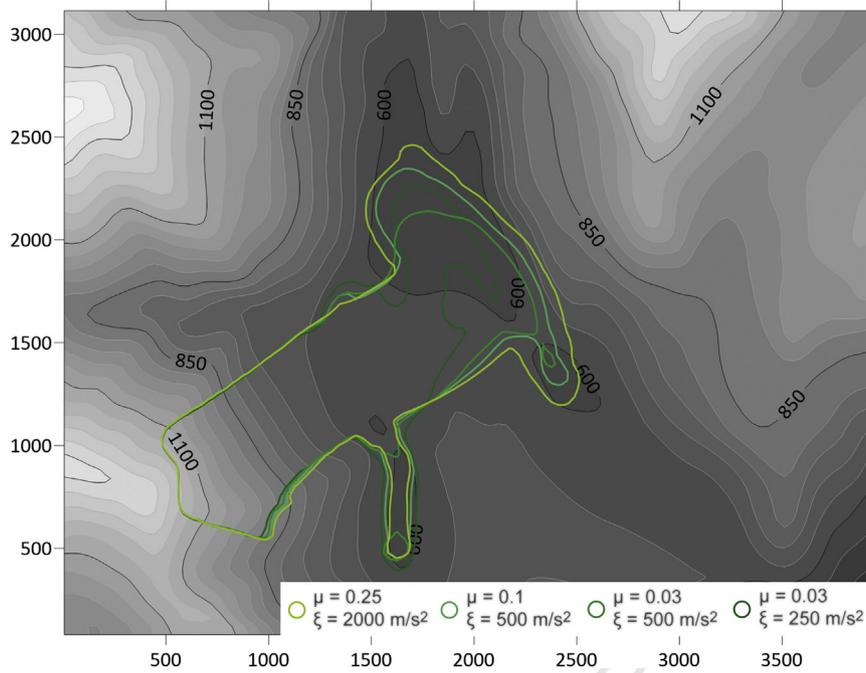


**Fig. 16.** The effect of friction and turbulence coefficients on impact area for the DAN3D Voellmy rheology glacial ice simulations, small volume (2.2 Mm<sup>3</sup>). Note that the green outlines are the maximum thickness = 2 m contours. Relative north and east scales (starting at 0 in the bottom left corner) are in metres. (For interpretation of the references to colour in this figure legend, the reader is referred to the web version of this article.)

595 because of the lowering of lake levels ascribable to regional climatic  
 596 changes (Biondi et al., 1981). This evidence is confirmed by a well-dated  
 597 and high-resolution record provided by a deep core from Lake Ledro  
 598 (southern Alps, Italy). Climate and land-use change (Joannin et al.,  
 599 2014) and flood frequency (Vannièrè et al., 2013) during the Holocene  
 600 were analyzed, together with fluctuations in lake level. Based on these  
 601 proxy data, some pieces of information can be used with reference to  
 602 the Tenno Lake paleoenvironmental evolution, because of the similarity  
 603 of geographical, geological, and geomorphological contexts. A low-stand  
 604 stage of the lake level, during the so-called Medieval Warm Period, was  
 605 followed by a rising trend, corresponding to the age of the submerged  
 606 forest. Therefore, no causal relationship exists between the Cima Salti  
 607 Landslide and the lake formation based on radiocarbon ages. Further-  
 608 more, no historical sources support the medieval hypothesis. The irregu-  
 609 lar distribution of landslide debris, and the lack thereof downstream of  
 610 the landslide source area, seems to suggest deposition from stagnant ice  
 611 (ice melting or downwasting in situ), rather than actively retreating ice,  
 612 which would have carried landslide material downstream.

613 Accepting that most of the deposits in the valley bottom are of glacial  
 614 origin, the most important aspect of the field investigations is the lack of

615 landslide evidence. This supports the following conclusions derived  
 616 from the simulations:

- The volume of the landslide is relatively small (2–5 Mm<sup>3</sup>). Thicknesses of  
 617 the deposit after coming to rest are not >20 m and more commonly  
 618 <10 m. 619
- The deposit travelled across stagnant glacial ice. This is supported by the  
 620 discontinuous distribution of landslide debris and the lack of landslide  
 621 debris downstream of the source area. If the landslide had runout onto  
 622 actively retreating ice or into the ice-free valley, we would expect to 623

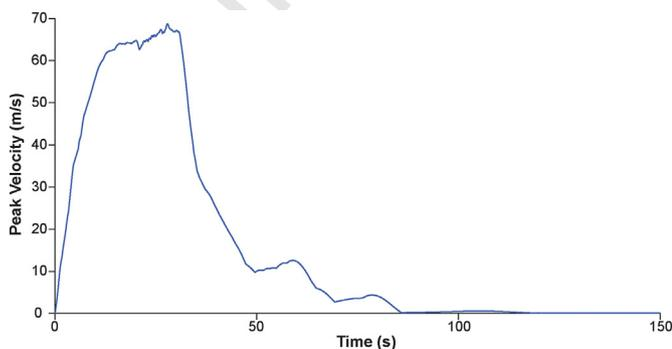


**Fig. 17.** Peak velocity plot for the DAN3D  $\varphi_b = 17^\circ$  simulation with glacial ice. Refer to Fig. 10 for comparison.

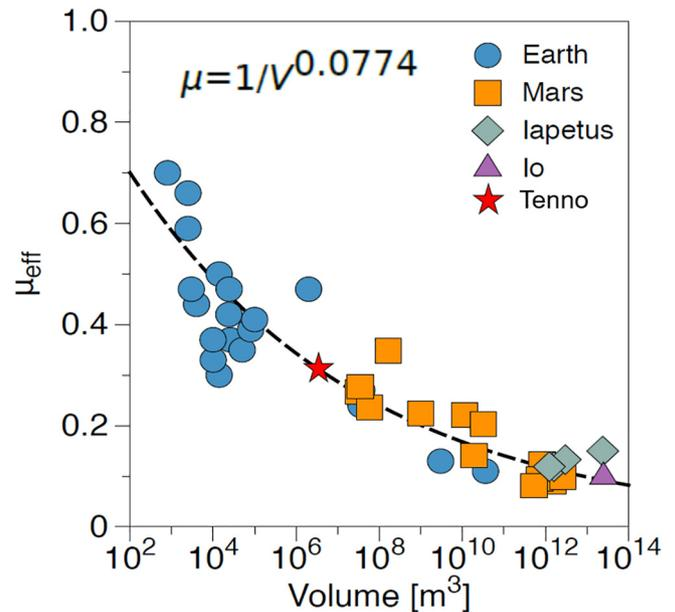


**Fig. 18.** Plot of empirical friction law, modified after Lucas et al. (2014). Cima Salti Landslide (Tenno) is represented by the red star. Only the small volume (2.2 Mm<sup>3</sup>) scenario is plotted, as it is considered most likely. (For interpretation of the references to colour in this figure legend, the reader is referred to the web version of this article.)

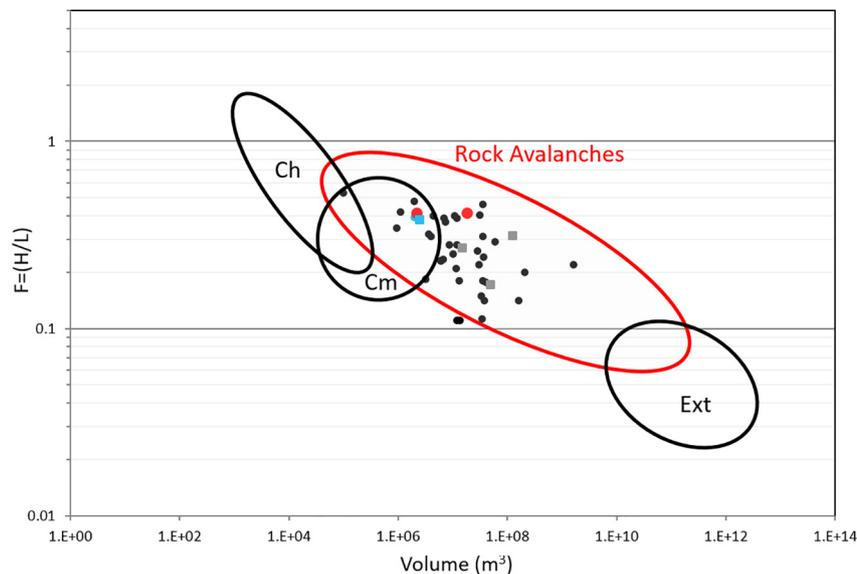


**Fig. 19.** Diagram relating the H/L ratio and the volume of different types of landslides (Ch = Chalk, Cm = coal mine waste, Ext = extra-terrestrial landslides). Red dots represent the Cima Salti Landslide with the two hypothesized volumes, black dots and grey squares represent, respectively, the rock avalanches analyzed with DAN3D and SHALTOP, described in literature and used as reference in the present work, blue square/dot represents the Thurwieser rock avalanche. (For interpretation of the references to colour in this figure legend, the reader is referred to the web version of this article.)

(Modified after Finlay et al., 1999).

624 find landslide debris downstream. Stagnant ice would have deposited  
625 the landslide debris haphazardly in the valley bottom as it melted,  
626 corresponding with the debris distribution observed in the field.  
627 • *The landslide did not dam a lake.* All lake sediments found in the valley  
628 were deposited in relation to glacial processes.

630 Our interpretation of the Cima Salti Landslide hence highlights the  
631 importance of careful field investigations, distinguishing similar  
632 deposits (till vs. landslide). Furthermore, the present work proves  
633 how numerical simulations can be used as a tool in understanding  
634 valley evolution and natural hazards. Implications for ancient landslides  
635 used as analogs in hazard assessments are significant.

## 636 Acknowledgments

637 This work has been partly funded by the ERC Contract No. ERC-CG-  
638 2013-PE10-617472 SLIDEQUAKES. We thank El Hadj Koné for his help  
639 in numerical simulations.

## 640 References

641 Alessio, M., Bella, F., Improta, S., Belluomini, G., Cortesi, C., Manelli, G., 1973. University of  
642 Rome carbon-14 dates XI. *Radiocarbon* 15 (2), 382–387.  
643 APPA, Trento Province, 2017. Piano di tutela delle acque.  
644 Bassetti, M., 1997. Studio geomorfologico sulle “Marocche” di Dro. *Studi Trentini di*  
645 *Scienze Naturali. Acta Geol.* 72, 5–30.  
646 Biondi, E., Pedrotti, F., Tommasi, G., 1981. Relitti di antiche foreste sul fondo di alcuni laghi  
647 del Trentino. *Studi Trentini di Scienze Naturali. Acta Biol.* 58, 93–117.  
648 Bouchut, F., Westdickenberg, M., 2004. Gravity driven shallow water models for arbitrary  
649 topography. *Commun. Math. Sci.* 2 (3), 359–389.  
650 Bouchut, F., Mangeney-Castelnau, A., Perthame, B., Vilotte, J.P., 2003. A new model of  
651 Saint-Venant and Savage-Hutter type for gravity-driven shallow water flows. *C.R.*  
652 *Math.* 336 (6), 531–536.  
653 Brunet, M., Le Friant, A., Boudon, G., Lafuerza, S., Talling, P., Hornbach, M., Ishizuka, O.,  
654 Lebas, E., Guyard, H., IODP Expedition 340 Science Party, 2016. Composition, geometry,  
655 and emplacement dynamics of a large volcanic island landslide offshore Martinique:  
656 from volcano flank-collapse to seafloor sediment failure? *Geochem. Geophys. Geosyst.*  
657 17 (3), 699–724.  
658 Brunet, M., Moretti, M., Le Friant, A., Mangeney, A., Fernandez-Nieto, E., Bouchut, F., 2017.  
659 Numerical simulation of the 30–45 ka debris avalanche flow of Montagne Pelée  
660 volcano, Martinique: from volcano flank-collapse to submarine emplacement  
661 comparison between measurements and numerical modelling. *Nat. Hazards* 87,  
662 1189–1222.

Campbell, C.S., Cleary, P.W., Hopkins, M., 1995. Large-scale landslide simulations: global  
663 deformation, velocities and basal friction. *J. Geophys. Res. Solid Earth* 100, 8267–8283.  
664 Castellarin, A., Picotti, V., 1990. Jurassic tectonic framework of the eastern border of the  
665 Lombardian basin. *Eclogae Geol. Helv.* 83 (3), 683–700.  
666 Chinaglia, N., 1993. Analisi geomeccanica di alcune grandi frane in unità calcaree  
667 stratificate: Le “Marocche” della bassa valle del Sarca. (Ph.D. Thesis). Università di  
668 Milano, Italy.  
669 Dalla Torre, K.W., 1913. *Tirol, Vorarlberg und Liechtenstein. Junk's Naturführer*, Berlin.  
670 Delaney, K.B., Evans, S.G., 2014. The 1997 Mount Munday landslide (British Columbia)  
671 and the behaviour of rock avalanches on glacier surfaces. *Landslides* 11, 1019–1036.  
672 Delannay, R., Valance, A., Mangeney, A., Roche, O., Richard, P., 2017. Granular and particle-  
673 laden flows: from laboratory experiments to field observations. *J. Phys. D: Appl. Phys.*  
674 50, 053001.  
675 Evans, S.G., Hungri, O., Clague, J.J., 2001. Dynamics of the 1984 rock avalanche and associ-  
676 ated distal debris flow on Mount Cayley, British Columbia, Canada; implications for  
677 landslide hazard assessment on dissected volcanoes. *Eng. Geol.* 61, 29–51.  
678 Farin, M., Mangeney, A., Roche, O., 2014. Dynamics, deposit and erosion processes in granu-  
679 lar collapse over sloping beds. *J. Geophys. Res. Earth Surf.* 119 (3), 504–532.  
680 Favreau, P., Mangeney, A., Lucas, A., Crosta, G., Bouchut, F., 2010. Numerical modeling of  
681 landquakes. *Geophys. Res. Lett.* 37, 1–5.  
682 Finlay, P.J., Mostyn, G.R., Fell, R., 1999. Landslide risk assessment: prediction of travel  
683 distance. *Can. Geotech. J.* 36, 556–562.  
684 Fuganti, A., 1969. Studio geologico di sei grandi frane nella regione Trentino Alto Adige.  
685 *Memorie del Museo Tridentino di Scienze Naturali.* 17 pp. 5–69.  
686 Galadini, F., Galli, P., Molin, D., Ciurletti, G., 2001. Searching for the source of the 1117  
687 earthquake in Northern Italy: a multidisciplinary approach. In: Glade, T., Albini, P.,  
688 Francés, F. (Eds.), *The Use of Historical Data in Natural Hazard Assessments*, Part A.  
689 Springer, Netherlands, pp. 3–27.  
690 Ghirotti, M., Picotti, V., Borgatti, L., Spreafico, M.C., Dolzan, S., 2015. Quaternary deposits  
691 around Lake Tenno (southwestern Trentino, Italy) document its glacial origin.  
692 *Rend. Online Soc. Geol. Ital.* 20, 162–165.  
693 Guidoboni, E., Comastri, A., Boschi, E., 2005. The “exceptional” earthquake of 3 January  
694 1117 in the Verona area (northern Italy): a critical time review and detection of  
695 two lost earthquakes (lower Germany and Tuscany). *J. Geophys. Res.* 110, B12309.  
696 Hart, M.W., Shaller, P.J., Farrand, T.G., 2012. When landslides are misinterpreted as faults:  
697 case studies from the Western United States. *Environ. Eng. Geosci.* 18 (4), 313–325.  
698 Hibert, C., Mangeney, A., Grandjean, G., Shapiro, N., 2011. Slopes instabilities in the  
699 Dolomieu crater, la Réunion island: from the seismic signal to the rockfalls character-  
700 istics. *J. Geophys. Res. Earth Surf.* 116, F04032.  
701 Hungri, O., Evans, S.G., 1996. Rock avalanche runout prediction using a dynamic model.  
702 *Proc. 7th International Symposium on Landslides*, Trondheim, Norway, pp. 233–238.  
703 Ivy-Ochs, S., Martin, S., Campedel, P., Hippe, K., Alfimov, V., Vockenhuber, C., Andreotti, E.,  
704 Carugati, G., Pasqual, D., Rigo, M., Viganò, A., 2017. Geomorphology and age of the  
705 Marocche di Dro rock avalanches (Trentino, Italy). *Quat. Sci. Rev.* 169, 188–205.  
706 Joannin, S., Magny, M., Peyron, O., Vannièrè, B., Galop, D., 2014. Climate and land-use  
707 change during the late Holocene at Lake Ledro (southern Alps, Italy). *The Holocene*  
708 24 (5), 591–602.  
709 Kuo, C.Y., Tai, Y.C., Bouchut, F., Mangeney, A., Pelanti, M., Chen, R.F., Chang, K.J., 2009. Sim-  
710 ulation of Tsoaling landslide, Taiwan, based on Saint Venant equations over general  
711 topography. *Eng. Geol.* 104, 181–189.  
712

- 713 Levy, C., Mangeney, A., Bonilla, F., Hibert, C., Calder, E.S., Smith, P.J., 2015. Friction weaken-  
714 ing in granular flows deduced from seismic records at the Soufrière Hills Volcano,  
715 Montserrat. *J. Geophys. Res. Solid Earth* 120, 7536–7557.
- 716 Lucas, A., Mangeney, A., Ampuero, J.P., 2014. Frictional velocity-weakening in landslides  
717 on Earth and on other planetary bodies. *Nat. Commun.* 5.
- 718 Mangeney, A., Bouchut, F., Thomas, N., Vilotte, J.P., Bristeau, M.O., 2007. Numerical model-  
719 ing of self-channeling granular flows and of their levee-channel deposits. *J. Geophys.*  
720 *Res.* 112, F02017.
- 721 Mangeney, A., Roche, O., Hungr, O., Mangold, Faccanoni, G., Lucas, A., 2010. Erosion and  
722 mobility in granular collapse over sloping beds. *J. Geophys. Res. Earth Surf.* 115,  
723 F03040.
- 724 Mangeney-Castelnaud, A., Bouchut, F., Vilotte, J.P., Lajeunesse, E., Aubertin, A., Pirulli, M.,  
725 2005. On the use of Saint Venant equations to simulate the spreading of a granular  
726 mass. *J. Geophys. Res.* 110, 17.
- 727 Martin, S., Campedel, P., Ivy-Ochs, S., Viganò, A., Alfimov, V., Vockenhuber, C., Andreotti, E.,  
728 Carugati, G., Pasqual, D., Rigo, M., 2014. Lavini di Marco (Trentino, Italy): <sup>36</sup>Cl  
729 exposure dating of a polyphase rock avalanche. *Quat. Geochronol.* 19, 106–116.
- 730 McColl, S., Davies, T., 2011. Evidence for a rock-avalanche origin for 'The Hillocks'  
731 "moraine", Otago, New Zealand. *Geomorphology* 127 (3), 216–224.
- 732 McDougall, S., Hungr, O., 2004. A model for the analysis of rapid landslide motion across  
733 three-dimensional terrain. *Can. Geotech. J.* 41, 1084–1097.
- 734 Moretti, L., Mangeney, A., Capdeville, Y., Stutzmann, E., Huggel, C., Schneider, D., Bouchut,  
735 F., 2012. Numerical modeling of the Mount Steller landslide flow history and of the  
736 generated long period seismic waves. *Geophys. Res. Lett.* 39, 1–7.
- 737 Moretti, L., Allstadt, K., Mangeney, A., Capdeville, Y., Stutzmann, E., Bouchut, F., 2015.  
738 Numerical modeling of the Mount Meager landslide constrained by its force history  
739 derived from seismic data. *J. Geophys. Res. Earth Surf.* 120, 2579–2599.
- 740 Orombelli, G., Sauro, U., 1988. I Lavini di Marco: un gruppo di frane oloceniche nel  
741 contesto morfotettonico dell'alta val Lagarina (Trentino). *Supplementi di Geografia*  
742 *Fisica e Dinamica Quaternaria.* 1 pp. 107–116.
- 743 Penck, A., Brückner, E., 1909. *Die Alpen im Eiszeitalter* (3 volumes). Tauchnitz, Leipzig.
- 744 Perna, G., 1974. *Le frane glaciali e postglaciali nel Trentino meridionale.* 22. Bollettino del  
745 Comitato Glaciologico Italiano, pp. 59–66.
- 746 Picotti, V., 2003. Note illustrative della carta geologica della Provincia di Trento alla scala  
747 1:25000 (Tavola 80 IV-Roncone). (105 pp.). SELCA, Firenze.
- 748 Picotti, V., Tommasi, G., 2002. Tavola 80 IV, Roncone: carta geologica della Provincia di  
749 Trento, scala 1:25000. SELCA, Firenze.
- 750 Pirocchi, A., 1992. Laghi di sbarramento per frana nelle Alpi: tipologia ed evoluzione. *Atti I*  
751 *convegno Nazionale Giovani Ricercatori in Geologia Applicata.* 93 pp. 128–136.
- 752 Pirulli, M., Mangeney, A., 2008. Results of back-analysis of the propagation of rock  
753 avalanches as a function of the assumed rheology. *Rock Mech. Rock. Eng.* 41, 59–84.
- Pirulli, M., Bristeau, M.O., Mangeney, A., Scavia, C., 2007. The effect of the earth pressure  
754 coefficients on the runout of granular material. *Environ. Model. Softw.* 22, 755  
756 1437–1454.
- 757 Reznichenko, N.V., Davies, T.R., 2015. The Gigantic Komansu Rock Avalanche Deposit in  
758 the Glaciated Alai Valley, Northern Pamir of Central Asia. In: Lollino, G., Giordan, D.,  
759 Crosta, G.B., Corominas, J., Azzam, R., Wasowski, J., Sciarra, N. (Eds.), *Engineering*  
760 *Geology for Society and Territory. Landslide Processes vol. 2.* Springer International  
761 Publishing, Cham, pp. 895–898.
- 762 Reznichenko, N.V., Davies, T.R., Shulmeister, J., Winkler, S., 2012. Influence of rock  
763 avalanches upon the formation of moraines and their subsequent palaeoclimatic  
764 interpretation: a critical appraisal. *Z. Geomorphol. Suppl. Issues* 56 (4), 37–54.
- 765 Schleier, M., Hermanns, R.L., Rohn, J., Gosse, J.C., 2015. Diagnostic characteristics and  
766 paleodynamics of supraglacial rock avalanches, Innerdalen, Western Norway.  
767 *Geomorphology* 245, 23–39.
- 768 Sosio, R., Crosta, G.B., Hungr, O., 2008. Complete dynamic modeling calibration for the  
769 Thurwieser rock avalanche (Italian Central Alps). *Eng. Geol.* 100, 11–26.
- 770 Sosio, R., Crosta, G.B., Chen, J.H., Hungr, O., 2012. Modelling rock avalanche propagation  
771 onto glaciers. *Quat. Sci. Rev.* 47, 23–40.
- 772 Tommasi, G., 1963. In: Manfrini, Monauni (Ed.), *I laghi del Trentino (Trento – Rovereto).*  
773 Tommasi, P., Verrucci, L., Campedel, P., Veronese, L., Pettinelli, E., Ribacchi, R., 2009.  
774 Buckling of high slopes: the case of Lavini di Marco (Trento-Italy). *Eng. Geol.* 109,  
775 93–108.
- 776 Trener, G.B., 1924. *Gli impianti idroelettrici della città di Trento, Geologia delle Marocche.*  
777 *Studi Trentini di Scienze Naturali.* 34(2) pp. 319–340.
- 778 Vaia, F., 1981. *La frana del lago di Tenno (Trentino).* *Studi Trentini di Scienze Naturali.* 58  
779 pp. 163–174.
- 780 Vanniè, B., Magny, M., Joannin, S., Simonneau, A., Wirth, S.B., Hamann, Y., Chapron, E.,  
781 Gilli, A., Desmet, M., Anselmetti, F.S., 2013. Orbital changes, variation in solar activity  
782 and increased anthropogenic activities: controls on the Holocene flood frequency in  
783 the Lake Ledro area, Northern Italy. *Clim. Past* 9 (3), 1193–1209.
- 784 Venzo, S., 1935. *Il Lago di Tenno: cenni geografico-geologici.* *Studi Trentini di Scienze*  
785 *Naturali.* 16 pp. 2–3.
- 786 Welkner, D., Eberhardt, E., Hermanns, R.L., 2010. Hazard investigation of the Portillo Rock  
787 Avalanche site, central Andes, Chile, using an integrated field mapping and numerical  
788 modelling approach. *Eng. Geol.* 114, 278–297.
- 789 Yamada, M., Mangeney, A., Matsushi, Y., Moretti, L., 2016. Estimation of dynamic friction  
790 of the Akatani landslide from seismic waveform inversion and numerical simulation.  
791 *Geophys. J. Int.* 206 (3), 1479–1486.
- 792 Yamada, M., Mangeney, A., Matsushi, Y., Matsuzawai, T., 2018. Estimation of Dynamic  
793 Friction and Movement History of Large Landslides, Landslides, Resubmitted After  
794 Review. 794

795